IMPACT LOAD IDENTIFICATION – FORENSIC ENGINEERING*

M. WIKLO, L. JANKOWSKI, J. HOLNICKI
Smart Technology Centre
Institute for Fundamental Technological Research
Polish Academy of Sciences
ul. Swietokrzyska 21, 00-049 Warszwa, Poland
E-mail: (mwiklo | ljank | holnicki)@ippt.gov.pl

1 SUMMARY

This paper presents a methodology for off-line impact load identification based on local strain and/or acceleration measurements. The motivation is stimulated by the need for effective post-crash analysis techniques, which would allow identification of the cause and the scenario of a collision (forensic engineering). On-board crash *Event Data Recorders* (so called *black boxes*) are now installed in many new cars, light trucks and buses. The devices record several crucial parameters such as speed of the vehicle, seat belt use, brake application etc. for up to 5 seconds before the impact [1, 2]. Currently more than 40 million cars are equipped with an EDR and the number is growing rapidly. The EDR-stored information allows to reconstruct the car motion in the last few seconds before the accident and during it [3, 4].

This paper proposes to equip the vehicle with additional devices measuring local strains and/or accelerations. The supplementary data obtained in this way can be stored along other data by the EDR for further analysis. The presented methodology can be used by forensic engineers to determine the evolution of the impact forces as well as the sequence of acting forces in the case of multiple impacts. The presented approach is fully applicable to all impact-exposed engineering structures.

2 PROBLEM FORMULATION

The method is based on the Virtual Distortion Method (VDM) [5] and is restricted to (both elastic and elasto-plastic) small deformation case. The identification task is formulated as an inverse problem. Therefore, the load identification procedure amounts to the minimisation of the objective function, which is proposed to be a weighted sum of the mean-square distances between the measured and modelled strains and accelerations. The VDM formulation allows to formulate the sensitivity analytically, thus fast-convergent gradient based optimisation techniques can be used. A similar approach has been also used in parallel research on structural adaptation to impact loads [6, 7].

2.1 Structural dynamic response

2.1.1 Displacements and strains

The VDM-based description of the dynamic response of an elasto-plastic truss structure can be applied to load identification [8]. The approach makes use of the so-called impulse influence matrices and discretises the continuous time into a finite number of discrete time steps denoted further on by t and τ. The development $u_i(t)$ of the displacement in the i-th degree of freedom of a truss structure, which has been loaded in degrees of freedom $\boldsymbol{L}$ and plastified in elements $\boldsymbol{\Xi}$ is expressed as follows:

* To appear in: *Proc. of the 2nd Int. Conf. on Nonsmooth Nonconvex Mechanics, NNMAE 2006.*

$$u_i(t)=\sum_{\tau=0}^{t}\sum_{n\in \boldsymbol{L}} D_{in}^{P}(t-\tau)\,p_n(\tau)+\sum_{\tau=0}^{t}\sum_{\xi\in \boldsymbol{\Xi}} D_{i\xi}^{\varepsilon}(t-\tau)\,\beta_{\xi}(\tau). \tag{1}$$

The Latin letters in Eq. (1) and thorough the paper denote the degrees of freedom, while the Greek letters are reserved for the truss elements. The corresponding strain evolution $\varepsilon_\alpha(t)$ can be calculated using a transformation matrix $\boldsymbol{G}$, whose elements are related to the direction cosines of the truss elements divided by their lengths, to take the form

$$\begin{aligned}\varepsilon_\alpha(t)&=\sum_{i=1}^{N} G_{\alpha i}\,u_i(t)\\ &=\sum_{\tau=0}^{t}\sum_{n\in \boldsymbol{L}} B_{\alpha n}^{P}(t-\tau)\,p_n(\tau)+\sum_{\tau=0}^{t}\sum_{\xi\in \boldsymbol{\Xi}} B_{\alpha\xi}^{\varepsilon}(t-\tau)\,\beta_{\xi}(\tau).\end{aligned} \tag{2}$$

In Eq. (1) and Eq. (2) $p_n(\tau)$ denotes the loading force acting in time step τ in the n-th degree of freedom, $\beta_\xi(\tau)$ denotes the plastic distortion generated in time step τ in the ξ-th element, and the matrices $\boldsymbol{D^P}$ and $\boldsymbol{D^\varepsilon}$, called the impulse (or dynamic) influence matrices, describe the discretised dynamic response of the structure to a unit impulse force and a unit distortion:

$D_{in}^{P}(\tau)$ is the displacement in time step τ in the i-th degree of freedom as a result of a unit impulse force applied in time step 0 in the n-th degree of freedom;

$D_{i\xi}^{\varepsilon}(\tau)$ is the displacement in time step τ in the i-th degree of freedom as a result of a unit distortion applied in time step 0 to the ξ-th element.

The transformation matrix $\boldsymbol{G}$ can be used to compute the matrices $\boldsymbol{B^P}$ and $\boldsymbol{B^\varepsilon}$, which occur in Eq. (2) and denote the strain evolution in time:

$B_{\alpha n}^{P}(\tau)$ is the strain in the element α in time step τ as a result of a unit impulse force applied in time step 0 in the n-th degree of freedom;

$B_{\alpha\xi}^{\varepsilon}(\tau)$ is the strain in the element α in time step τ as a result of a unit distortion applied in time step 0 to the ξ-th element.

The unit force and the unit distortion, which generate the dynamic influence matrices, last for one time step only and model in fact the Dirac type of impulse. Their elements can be determined by numerical integration of the equations of motion. Eq. (1) and Eq. (2) represent the overall response of the structure as a simple superposition of the responses to the loadings occurring in all previous time steps. Notice also that the dynamic influence matrices retain full information about the modelled structure, including the boundary conditions.

The elasto-plastic physical properties are described by the piecewise linear relation depicted in Fig. 1. The stress $\sigma_\alpha(t)$ in a plastified element α in time t can be expressed in terms of the current value of the plastic distortion $\beta_\alpha(t)$ as well as in terms of the yield level $\sigma^* = E_\alpha \varepsilon^*$ and the hardening coefficient γ_α

$$\sigma_\alpha(t)=E_\alpha\left[\varepsilon_\alpha(t)-\beta_\alpha(t)\right], \tag{3}$$

$$\sigma_\alpha(t)\mp\sigma^*=E_\alpha\gamma_\alpha\left[\varepsilon_\alpha(t)\mp\varepsilon_\alpha^*\right], \tag{4}$$

where the choice of the sign depends on the stress sign. Combined together they yield

$$\beta_\alpha(t)=(1-\gamma_\alpha)\left[\varepsilon_\alpha(t)\mp\varepsilon_\alpha^*\right], \tag{5}$$

where the strain $\varepsilon_\alpha(t)$ is expressed by Eq. (2). If the elements of the matrices $\boldsymbol{B^P}$ and $\boldsymbol{B^\varepsilon}$ occurring in Eq. (2) are all zero at time step 0, then the plastic distortion $\beta_\alpha(t)$ occurs only on

the left hand side of Eq. (5), and thus can be directly computed if the yield stress level has been exceeded, time step by time step. This amounts to the assumption that a force acting in time step τ results in strains/displacements first in the next time step. Otherwise Eq. (5) (rewritten for all plastified elements α) can be transformed to a set of linear equations in unknowns $\beta_\alpha(t)$ and solved using standard linear methods, time step by time step.

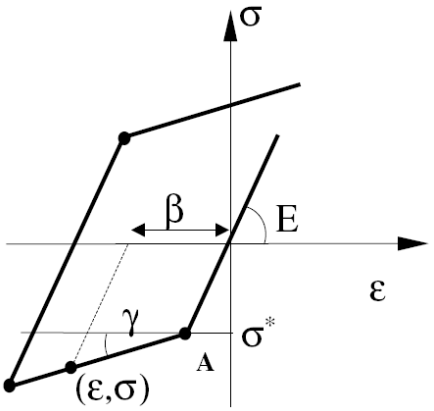

Fig. 1 Piecewise linear constitutive relation

2.1.2 Velocities and accelerations

The identification task requires comparison of calculated and measured quantities. The strains can be both easily computed with Eq. (2) and measured with strain gauges. On the other hand, although Eq. (1) directly expresses the displacements for calculations, in a real-world structure it is much easier to measure the accelerations.

The nodal velocities and accelerations can be expressed by direct differentiation of Eq. (1). In an obvious analogy to a continuous-time system

$$\begin{aligned}\dot{u}_i(t) = &\frac{1}{\Delta t}\sum\nolimits_{n\in L} D^P_{in}(0)\, p_n(t) + \frac{1}{\Delta t}\sum\nolimits_{n\in L} D^\varepsilon_{i\xi}(0)\,\beta_\xi(t) \\ &+ \sum\nolimits^t_{\tau=0}\sum\nolimits_{n\in L} \dot{D}^P_{in}(t-\tau)\, p_n(\tau) + \sum\nolimits^t_{\tau=0}\sum\nolimits_{\xi\in\Xi} \dot{D}^\varepsilon_{i\xi}(t-\tau)\,\beta_\xi(\tau)\end{aligned} \tag{6}$$

and

$$\begin{aligned}\ddot{u}_i(t) = &\frac{1}{\Delta t}\sum\nolimits_{n\in L} D^P_{in}(0)\, \dot{p}_n(t) + \frac{1}{\Delta t}\sum\nolimits_{n\in L} D^\varepsilon_{i\xi}(0)\,\dot{\beta}_\xi(t) \\ &+ \frac{1}{\Delta t}\sum\nolimits_{n\in L} \dot{D}^P_{in}(0)\, p_n(t) + \frac{1}{\Delta t}\sum\nolimits_{n\in L} \dot{D}^\varepsilon_{i\xi}(0)\,\beta_\xi(t) \\ &+ \sum\nolimits^t_{\tau=0}\sum\nolimits_{n\in L} \ddot{D}^P_{in}(t-\tau)\, p_n(\tau) + \sum\nolimits^t_{\tau=0}\sum\nolimits_{\xi\in\Xi} \ddot{D}^\varepsilon_{i\xi}(t-\tau)\,\beta_\xi(\tau).\end{aligned} \tag{7}$$

Eq. (6) allows direct computations of the nodal velocities. Unfortunately, Eq. (7) contains two troublesome components: the derivatives with respect to time of the acting force $\partial p_n(t)/\partial t$ and of the plastic distortion $\partial\beta_\alpha(t)/\partial t$. A more convenient formula can be obtained by mixing the VDM formulation of Eq. (1) and Eq. (6) with the Newmark's integration scheme [9]. In each time step the displacements and the velocities can be calculated using the formulae Eq. (1) and Eq. (6), but the accelerations are computed according to the Newmark's formula:

$$\ddot{u}_i(t) = a_0\big[u_i(t) - u_i(t-1)\big] - a_2\dot{u}_i(t-1) - a_3\ddot{u}_i(t-1)\,, \tag{8}$$

where the coefficients a_0, a_2 and a_3 denote constant Newmark's integration parameters.

2.2 Objective function

The aim is to determine the time evolution of the loading forces $p_n(t)$ that minimises the discrepancy between the measured and calculated structure behaviour. Each unknown $p_n(t)$ denotes the loading force, which acts in time step t in the n-th degree of freedom, hence all $p_n(t)$ become (large in number) arguments of the objective function.

In comparison with the previous research [8, 10] this paper proposes a more complicated form of the objective function, which is composed here of two weighted terms to use both strains and accelerations:

$$f(\boldsymbol{p}) = f_1(\boldsymbol{p}) + f_2(\boldsymbol{p}), \tag{9}$$

where f_1 represents the scaled mean square distance between the locally measured $\varepsilon_\alpha^M(t)$ and the calculated $\varepsilon_\alpha(t)$ strains, while f_2 represents the scaled mean square distance between the locally measured $\ddot{u}_n^M(t)$ and the calculated $\ddot{u}_n(t)$ accelerations:

$$f_1(\boldsymbol{p}) = \frac{\sum_{t=0}^{T} \sum_{\alpha \in \boldsymbol{\Sigma}} \left[\varepsilon_\alpha^M(t) - \varepsilon_\alpha(t)\right]^2}{\sum_{t=0}^{T} \sum_{\alpha \in \boldsymbol{\Sigma}} \left[\varepsilon_\alpha^M(t)\right]^2}, \tag{10}$$

$$f_2(\boldsymbol{p}) = \frac{\sum_{t=0}^{T} \sum_{i \in \boldsymbol{A}} \left[\ddot{u}_i^M(t) - \ddot{u}_i(t)\right]^2}{\sum_{t=0}^{T} \sum_{i \in \boldsymbol{A}} \left[\ddot{u}_i^M(t)\right]^2}. \tag{11}$$

The weighting denominators in Eq. (10) and Eq. (11) are necessary to balance the influence of both components on the overall objective function f. The set of elements equipped with strain gauges is denoted by $\boldsymbol{\Sigma}$, while $\boldsymbol{A}$ denotes the the set of nodes equipped with accelerometers.

2.3 Gradients

The strength of the VDM approach lies in the analytically expressible gradient of the objective function Eq. (9). At the current stage of the research the computations in the plastic case would require calculating and memorising a huge number of approx. $T^3 \cdot |\boldsymbol{L}| \cdot |\boldsymbol{\Sigma}| \cdot |\boldsymbol{\Xi}|$ gradient components, where T is the number of time steps, $|\boldsymbol{L}|$ is the number of the loaded degrees of freedom, $|\boldsymbol{\Sigma}|$ is the number of strain gauges and $|\boldsymbol{\Xi}|$ is the number of plastified elements. Therefore, this paper is limited to the case of elastic truss structures only.

The derivative of the objective function Eq. (9) with respect to the unknown force $p_n(\tau)$ acting in time step τ in the n-th degree of freedom,

$$\begin{aligned} \frac{\partial f(\boldsymbol{p})}{\partial p_n(\tau)} = &-2\left[\sum_{t=0}^{T} \sum_{\alpha \in \boldsymbol{\Sigma}} \left[\varepsilon_\alpha^M(t)\right]^2\right]^{-1} \sum_{t=0}^{T} \sum_{\alpha \in \boldsymbol{\Sigma}} \left[\varepsilon_\alpha^M(t) - \varepsilon_\alpha(t)\right] \frac{\partial \varepsilon_\alpha(t)}{\partial p_n(\tau)} \\ &-2\left[\sum_{t=0}^{T} \sum_{i \in \boldsymbol{A}} \left[\ddot{u}_i^M(t)\right]^2\right]^{-1} \sum_{t=0}^{T} \sum_{i \in \boldsymbol{A}} \left[\ddot{u}_i^M(t) - \ddot{u}_i(t)\right] \frac{\partial \ddot{u}_i(t)}{\partial p_n(\tau)}, \end{aligned} \tag{12}$$

is expressed in terms of the corresponding derivatives of the calculated strains $\varepsilon_\alpha(t)$ and accelerations $\ddot{u}_i(t)$, which in the elastic case can be calculated by differentiation of Eq. (2),

$$\frac{\partial \varepsilon_\alpha(t)}{\partial p_n(\tau)} = B^P_{\alpha n}(t-\tau)\cdot \mathbf{1}_{\{\tau \leqslant t\}}, \tag{13}$$

and by iterative application of differentiated Eq. (8), Eq. (6) and Eq. (1),

$$\frac{\partial \ddot{u}_i(t)}{\partial p_n(\tau)} = \begin{array}{l} a_0 D^P_{in}(0)\cdot \mathbf{1}_{\{\tau = t\}} \quad \text{for} \quad t \leqslant \tau, \\ -a_0(1+a_3) D^P_{in}(0) + \left(a_0 - \dfrac{1}{\Delta t} a_2\right) D^P_{in}(1) - a_2 \dot{D}^P_{in}(1) \quad \text{for } t=\tau+1, \\ a_0\left[D^P_{in}(t-\tau) - D^P_{in}(t-1-\tau)\right] \\ \qquad -a_2 \dot{D}^P_{in}(t-1-\tau) - a_3 \dfrac{\partial \ddot{u}_i(t-1)}{\partial p_n(\tau)} \quad \text{for } t>\tau+1. \end{array} \tag{14}$$

3 OPTIMISATION

An effective, fast-converging optimisation procedure has been derived and tested for the objective function f_1 of Eq. (10). This is not a straightforward task even in the reported elastic case, as the number of variables $p_n(\tau)$ is significant (2,000 in the example considered below). The procedure is based on the fact that the calculated strain $\varepsilon_\alpha(t)$ expressed in Eq. (2) is a linear combination of $p_n(\tau)$, hence the objective function f_1 of Eq. (10) is a (convex) *quadratic function* of its arguments and can be exactly expanded around a given force vector $\boldsymbol{p}=\langle p_n(\tau)\rangle$

$$f_1(\boldsymbol{p}+\boldsymbol{d}) = f_1(\boldsymbol{p}) + \nabla f_1(\boldsymbol{p})^T \boldsymbol{d} + \frac{1}{2}\boldsymbol{d}^T \boldsymbol{H}\, \boldsymbol{d}, \tag{15}$$

where $\boldsymbol{H}$ is the (constant and positive semidefinite) Hessian of f_1. This observation leads to effective formulae for line minimisation of f_1 and determination of the conjugated directions. The following formulae can be derived by equating Eq. (15) with Eq. (10) and Eq. (2):

$$\begin{aligned} \nabla f_1(\boldsymbol{p})^T \boldsymbol{d} &= -2C_{scl} \sum_{t=0}^{T} \sum_{\alpha \in \Sigma} \varepsilon^{(\boldsymbol{d})}_\alpha(t)\left[\varepsilon^M_\alpha(t) - \varepsilon^{(\boldsymbol{p})}_\alpha(t)\right], \\ \boldsymbol{d}^T \boldsymbol{H}\, \boldsymbol{d} &= 2C_{scl} \sum_{t=0}^{T} \sum_{\alpha \in \Sigma} \left[\varepsilon^{(\boldsymbol{d})}_\alpha(t)\right]^2, \end{aligned} \tag{16}$$

where C_{scl} denotes the scaling coefficient of the objective function f_1 (the inverse of the denominator in Eq. (10)), and $\varepsilon^{(\boldsymbol{p})}_\alpha(t)$, $\varepsilon^{(\boldsymbol{d})}_\alpha(t)$ denote the strains calculated with Eq. (2) for the loading forces $\boldsymbol{p}=\langle p_n(\tau)\rangle$ and $\boldsymbol{d}=\langle d_n(\tau)\rangle$, respectively.

3.1 Line optimisation

Even for relatively simple structures the Hessian occurring in Eq. (15) is too large to compute and invert it in a reasonable time and in a numerically stable way, which is necessary to find the minimum in one step only (the Newton method). Therefore, a series of line optimisations has to be performed; each step amounts to finding at a given point $\boldsymbol{p}$ the line minimum along a direction $\boldsymbol{d}$, i.e. the value of s that minimises

$$f_1(\boldsymbol{p}+s\cdot\boldsymbol{d}) = f_1(\boldsymbol{p}) + s\cdot\nabla f_1(\boldsymbol{p})^T \boldsymbol{d} + s^2\cdot\frac{1}{2}\boldsymbol{d}^T \boldsymbol{H}\, \boldsymbol{d}, \tag{17}$$

which is a simple convex quadratic function of s with the minimum at

$$s_{min} = -\frac{\nabla f_1(\boldsymbol{p})^T \boldsymbol{d}}{\boldsymbol{d}^T \boldsymbol{H}\, \boldsymbol{d}} = \frac{\sum_{t=0}^{T} \sum_{\alpha \in \Sigma} \varepsilon_\alpha^{(\boldsymbol{d})}(t) \left[\varepsilon_\alpha^M(t) - \varepsilon_\alpha^{(\boldsymbol{p})}(t) \right]}{\sum_{t=0}^{T} \sum_{\alpha \in \Sigma} \left[\varepsilon_\alpha^{(\boldsymbol{d})}(t) \right]^2}. \tag{18}$$

3.2 Conjugated directions

The steepest descent method takes at each optimisation step $\boldsymbol{d} = -grad\, f_1(\boldsymbol{p})$ in Eq. (17) but it suffers from slow convergence. On the contrary, because the objective function f_1 is quadratic and the Hessian $\boldsymbol{H}$ is constant, choosing in each step a direction $\boldsymbol{d}_{n+1}$ *conjugated* with all/few previous directions $\boldsymbol{d}_{n-k}$, ..., $\boldsymbol{d}_n$ allows to go by Eq. (18) directly to the minimum in the whole subspace generated by all considered directions $\boldsymbol{d}_{n-k}$, ..., $\boldsymbol{d}_n$, $\boldsymbol{d}_{n+1}$. Therefore, starting with the steepest descent direction and making use of the conjugacy criterion $\boldsymbol{d}_i^T \boldsymbol{H} \boldsymbol{d}_j = 0$,

$$\boldsymbol{d}_{n+1} = -\nabla f_1(\boldsymbol{p}_{n+1}) + \sum_{i=0}^{k} \eta_{n-i} \boldsymbol{d}_{n-i}, \quad \text{where} \quad \eta_i = \frac{\nabla f_1(\boldsymbol{p}_{n+1})^T \boldsymbol{H}\, \boldsymbol{d}_i}{\boldsymbol{d}_i^T \boldsymbol{H}\, \boldsymbol{d}_i}. \tag{19}$$

3.3 The algorithm

The most expensive operations in the algorithm below are the calculations of the gradients (Eq. (12), Eq. (13)) and of the response (Eq. (2)), marked with the asterisk below: both require four internal loops. All other operations require only two loops and are much faster.

Initial calculations:

initialise: $\boldsymbol{p}_0 = \boldsymbol{0}$ and $\varepsilon_\alpha^{(\boldsymbol{p}_0)}(t) = \boldsymbol{0}$
(*)calculate $\boldsymbol{d}_0 = -\nabla f_1(\boldsymbol{p}_0)$ and $\varepsilon_\alpha^{(\boldsymbol{d}_0)}(t)$
normalise: $D = \sqrt{\boldsymbol{d}_0^T \boldsymbol{H}\, \boldsymbol{d}_0}$, $\boldsymbol{d}_0 = \boldsymbol{d}_0 / D$ and $\varepsilon_\alpha^{(\boldsymbol{d}_0)}(t) = \varepsilon_\alpha^{(\boldsymbol{d}_0)}(t) / D$
calculate the line minimum $s = -\nabla f_1(\boldsymbol{p}_0)^T \boldsymbol{d}_0$
store $\boldsymbol{d}_0$ and $\varepsilon_\alpha^{(\boldsymbol{d}_0)}(t)$

The loop:

update: $\boldsymbol{p}_{n+1} = \boldsymbol{p}_n + s \cdot \boldsymbol{d}_n$ and $\varepsilon_\alpha^{(\boldsymbol{p}_{n+1})}(t) = \varepsilon_\alpha^{(\boldsymbol{p}_n)}(t) + s \cdot \varepsilon_\alpha^{(\boldsymbol{d}_n)}(t)$
(*)calculate $\boldsymbol{d}_{n+1} = -\nabla f_1(\boldsymbol{p}_{n+1})$ and $\varepsilon_\alpha^{(\boldsymbol{d}_{n+1})}(t)$
conjugate direction: for (i = 0; i <= k; ++i)
$\eta = -\boldsymbol{d}_{n+1}^T \boldsymbol{H}\, \boldsymbol{d}_{n-i}$
$\boldsymbol{d}_{n+1} = \boldsymbol{d}_{n+1} + \eta \cdot \boldsymbol{d}_{n-i}$, $\varepsilon_\alpha^{(\boldsymbol{d}_{n+1})}(t) = \varepsilon_\alpha^{(\boldsymbol{d}_{n+1})}(t) + \eta \cdot \varepsilon_\alpha^{(\boldsymbol{d}_{n-i})}(t)$
normalise: $D = \sqrt{\boldsymbol{d}_{n+1}^T \boldsymbol{H}\, \boldsymbol{d}_{n+1}}$, $\boldsymbol{d}_{n+1} = \boldsymbol{d}_{n+1} / D$ and $\varepsilon_\alpha^{(\boldsymbol{d}_{n+1})}(t) = \varepsilon_\alpha^{(\boldsymbol{d}_{n+1})}(t) / D$
calculate the line minimum $s = -\nabla f_1(\boldsymbol{p}_{n+1})^T \boldsymbol{d}_{n+1}$
store $\boldsymbol{d}_{n+1}$ and $\varepsilon_\alpha^{(\boldsymbol{d}_{n+1})}(t)$

3.4 Solution ambiguity

Minimisation of the objective function f_1 corresponds in fact to solving the linear system given by Eq. (2) with the left hand side replaced by the measured strains $\varepsilon_\alpha^M(t)$. Therefore, provided the system is not singular, to guarantee the uniqueness of the solution, the number of unknowns must not exceed the number of equations, i.e. there must be at least as much strain gauges $|\boldsymbol{\Sigma}|$ as the loaded degrees of freedom $|\boldsymbol{L}|$. Otherwise there would exist a whole subspace of feasible solutions, which result in the same measured strain evolutions.

4 NUMERICAL EXAMPLE

Fig. 2 shows the modelled elastic truss structure. It is 4 m long; the elements are 10 mm^2 in cross-section, 0.5 m or $0.5\sqrt{2}$ m long, and made of steel (7,800 kg/m^3; 200 GPa). Eight strain gauges were located in the eight diagonal elements of the bottom plane. The two most

left hand side nodes were deprived of all degrees of freedom, while the two most right hand side nodes were free in the longitudinal direction only (i.e. along the structure).

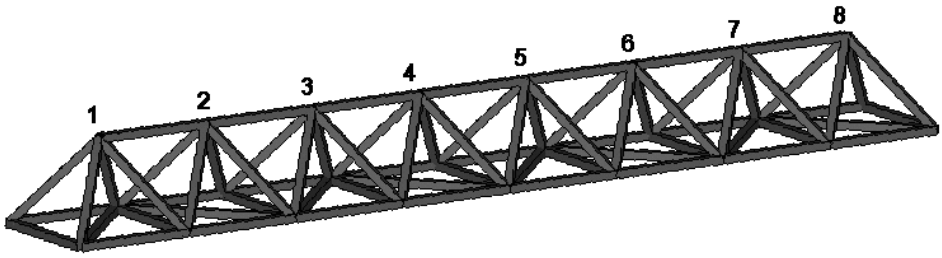

Fig. 2 Elastic truss structure modelled in the numerical example

4.1 Modelled impact forces and measurements

The modelled loadings, which are to be identified, were assumed to be triangular in shape and occur vertically in the 3rd and 4th node, see Fig. 3 (left). The response of the structure has been calculated; the responses of the eight strain gauges modelling the measurements $\varepsilon_\alpha^M(t)$ have been stored, see Fig. 3 (right) for three examples (the gauges are numbered from left to right).

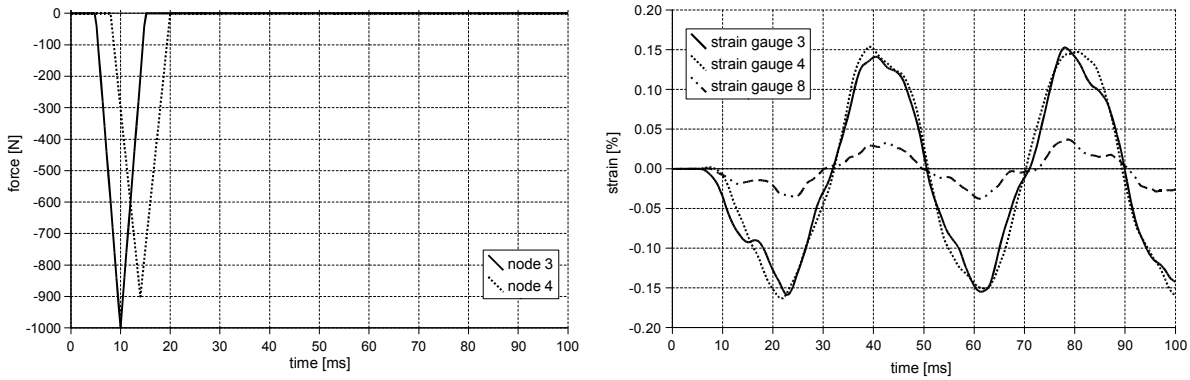

Fig. 3 Modelled impact forces (left) and the corresponding measurements of three sample strain gauges (right)

4.2 Load identification

As there are eight strain gauges, force evolution in eight degrees of freedom can be identified. Therefore, it was assumed that vertical loading can occur in the nodes 1 to 8. The simulation time was 100 ms, divided into 250 time steps. 1,000 optimisation steps have been made.

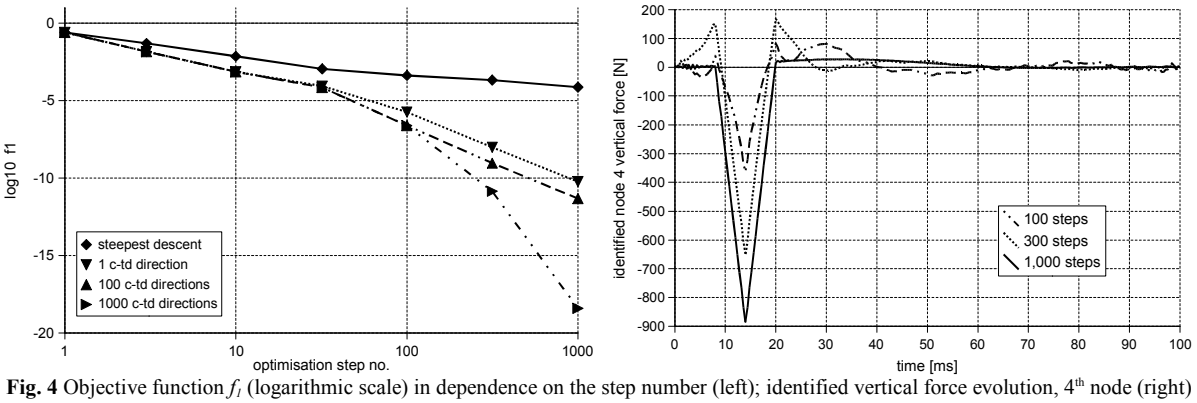

Fig. 4 Objective function f_1 (logarithmic scale) in dependence on the step number (left); identified vertical force evolution, 4th node (right)

Fig. 4 (left) shows in the logarithmic scale the value of the objective function in dependence on the optimisation step number in the case of 0 (steepest descent), 1, 100 and 1,000 (all) conjugated directions remembered. An average time per optimisation step (calculated after 1,000 steps) was 115 ms, 118 ms, 142 ms and 211 ms, respectively. The identified vertical

force evolution in the 4th node after 100, 300 and 1,000 optimisation steps is shown in Fig. 4 (right), all calculated in the case of 1,000 (all) conjugated directions remembered.

5 FURTHER WORK

Further research is planned to involve also accelerations in the process, investigate the sensitivity to measurement noise, devise robust optimisation heuristics, include the elasto-plastic case and investigate the issue of the best sensor locations. In parallel, an experimental verification with the truss structure depicted in Fig. 2 is currently being prepared.

6 CONCLUSIONS

A promising and robust methodology for post-accident impact load identification is proposed. It is based on local measurements, which can be stored in on-board Event Data Recorders (black boxes), and is fully applicable to all impact-exposed engineering structures. The intended application area is forensic engineering, where the technique can have important implications for the vehicle design industry and for the insurance sector, as effective determination of accident scenario is crucial in reducing costs of automobile insurance.

7 ACKNOWLEDGEMENT

The authors gratefully acknowledge the financial support through the Polish Research Projects MAT-INT (PBZ-KBN-115/T08/2004) and DIADYN (PBZ-KBN-105/T10/2003).

8 REFERENCES

[1] T. M. Kowalick, *Fatal Exit: The Automotive Black Box Debate*, Wiley-IEEE Press, November 2004.

[2] H. C. Gabler, D. J. Gabauer, H. L. Newell, M. E. O'Neill, NCHRP Web-Only Document #75: *Use of Event Data Recorder (EDR) Technology for Highway Crash Data Analysis*, December 2004.

[3] M. Guzek, Z. Lozia, *Rekonstrukcja trajektorii ruchu pojazdu na podstawie zapisów 'czarnych skrzynek' - badania symulacyjne*, Zeszyty Naukowe Instytutu Pojazdów, Vol. 57. No. 2, 2005.

[4] M. Guzek, Z. Lozia, *Possible Errors Occurring During Accident Reconstruction Based on Car "Black Box" Records*, SAE 2002 World Congress & Exhibition, 4-7 March, Detroit, Michigan, 2002.

[5] T. G. Zielinski, *Metoda impulsowych dystorsji wirtualnych z zastosowaniem do modelowania i identyfikacji defektów w konstrukcjiach*, Ph.D. thesis, Institute of Fundamental Technological Research PAS, Warsaw, 2004.

[6] J. Holnicki-Szulc, M. Wiklo, *Adaptive Impact Absorbers: the Concept, Design Tools and Applications*, Proc. Of the 3rd World Conf. on Struct. Control, Como, Italy, 2002.

[7] J. Holnicki-Szulc, P. Pawlowski, M. Wiklo, *High-performance impact absorbing materials - the concept, design tools and applications*, Smart Materials and Structures, Vol. 12, No. 3, 2003.

[8] M. Wiklo, J. Holnicki-Szulc, *Local measurements based impact loads identification*, Proc. of the 6th Int. Conf. on Damage Assessment of Structures, DAMAS, 4-6 July, Gdansk, Poland, 2005.

[9] K. Bathe, *Finite Element Procedures in Engineering Analysis*, Prentice-Hall, Inc., Englewood Cliffs, 1982.

[10] A. Swiercz, P. Kołakowski, J. Holnicki-Szulc, *Damage identification through frequency-based analysis for steady-state dynamic responses*, Proc. of the II ECCOMAS Thematic Conference on Smart Structures and Materials, SMART'05, 18-21 July, Lisboa, Portugal, 2005.